

A Digital Microfluidic Platform for the Microscale Production of Functional Immune Cell Therapies

Samuel R. Little, Niloufar Rahbari, Mehri Hajiaghayi, Fatemeh Gholizadeh, Fanny-Mei Cloarec-Ung, Joel Phillips, Hugo Sinha, Alison Hirukawa, David J.H.F. Knapp, Peter J. Darlington, and Steve C. C. Shih*



Cite This: *Anal. Chem.* 2025, 97, 11026–11034



Read Online

ACCESS |



Metrics & More

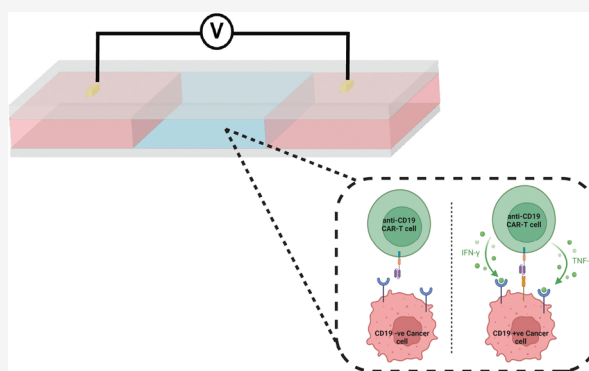


Article Recommendations



Supporting Information

ABSTRACT: Genetically engineering human immune cells has been shown to be an effective approach for developing novel cellular therapies to treat a wide range of diseases. To expand the scope of these cellular therapies while solving persistent challenges, extensive research and development is still required. Here we use a digital microfluidic enabled electroporation system (referred to as triDrop) specifically designed to mitigate harm during electroporation procedures and compare against two state-of-the-art commercially available systems for the engineering of primary human T cells. We describe the ability to use triDrop for highly efficient transfection with minimal reagent consumption while preserving a healthy transcriptomic profile. Finally, we show for the first time the ability to use a digital microfluidic platform for the miniaturized production of Chimeric Antigen Receptor (CAR) T cell therapies demonstrating how this novel system can lead to a 2-fold improvement in immunotherapeutic functionality compared to gold standard methods while providing up to a 20-fold reduction in cost. These results highlight the potential power of this system for automated, rapid, and affordable next-generation cell therapy R&D.



Reprogramming the functionality of human T cells by inserting novel biological payloads has been shown to be a promising avenue of therapeutic development.¹ Removing immune cells from a patient, modifying the cells, and reinjecting them into the patient is a viable treatment for hematological^{2–4} and solid cancers.⁵ However, manufacturing of these therapies is challenging,¹ and current therapies can lack specificity.⁶ Efforts have been made to engineer immune cells to avoid so-called “on-target, off-tumor” toxicities.⁷ However, developing cellular therapies for cancer that is affordable, as well as safe and efficient will require additional complex genetic engineering and substantial research and development (R&D).^{8,9}

Given that preclinical R&D is a substantial driver of cost and time when bringing cell therapy to market,¹⁰ a platform capable of automating laborious payload delivery procedures and processing numerous samples in parallel, while requiring only small inputs of cell and reagents per reaction could reduce the cost and length of many cellular therapy development programs. Currently, there are several popular commercially available platforms used for cell therapy R&D; however, these platforms either require performing each reaction serially (one-at-a-time) for testing multiple conditions¹¹ or require large cellular and reagent inputs.¹²

Microfluidic-based platforms are emerging as technologies for the physical transfection of human immune cells using techniques such as mechanical squeezing or compression,^{13–17} fluidic shearing,^{18,19} and electroporation.^{20,21} More generally, microfluidic technologies have emerged as a transformative approach for the production of CAR T cell therapies.²² A primary goal for this field has been to develop a platform capable of efficiently inserting a single type of payload into cells while operating continuously with a throughput >10⁶ cells/min.²³ While these are important techniques for clinical-scale manufacturing,²⁴ we are not currently aware of a robust, parallel microfluidics platform capable of R&D scale transfection where performing many small reactions is prioritized.

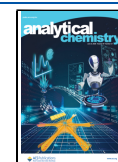
In recent years, electroporation (EP) has become a widely used technique for transfection due to its versatility and relative ease of use.²⁵ However, substantial concerns have been

Received: December 19, 2024

Revised: May 12, 2025

Accepted: May 12, 2025

Published: May 20, 2025



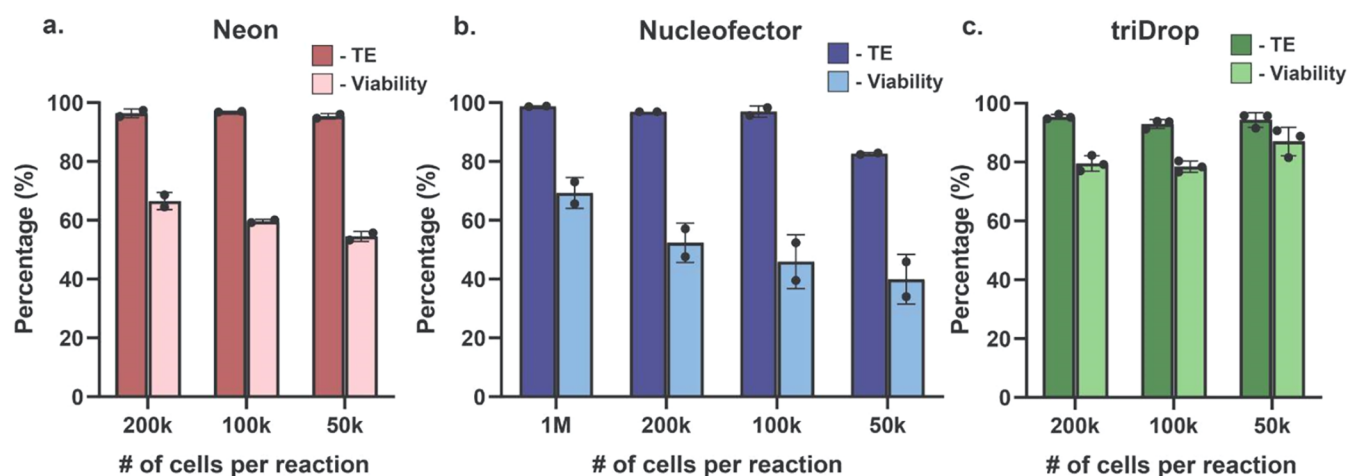


Figure 1. Three electroporation systems. Bar graphs depicting transfection efficiency (TE; dark colors) and viability (light colors) when performing electroporation using varying numbers of cells per reaction in technical duplicates for (a) Neon, (b) Nucleofector, and technical triplicates for (c) triDrop.

raised regarding cellular dysfunction emerging from cells engineered via EP where harmful side effects from the pore-generating process can lead to cells with poor viability, genetic dysregulation, and lacking core functionalities.^{23,26,27} These side effects include excessive current generation during electrical pulsing leading to joule heating,²⁸ and electrolytic reactions at the anode and cathode causing a pH change and metal contaminants in the EP media interacting with cells.^{29,30} An ideal microfluidic platform for cell therapy R&D would not only efficiently engineer cells but would also preserve the viability and functionality of those cells for use and analysis in functional assays.

We previously published a novel three-droplet system (referred to as triDrop) that allowed for efficient EP of human T cells on a digital microfluidic (DMF) platform.³¹ Here, we describe how triDrop efficiently transfects reduced amounts of cells while using less payload compared to two commercially available alternatives, allowing for rapid and affordable cell engineering while preserving healthy transcriptomic profiles. We then show for the first time the use of a DMF platform for the miniaturized production of functional immune cell therapies. Using our platform, we achieved the same delivery efficiency as gold standard methods but, by preserving cell health, we were able to generate cells that could perform up to 2-fold more effectively when mounting an immune response against cancer cells. Taken together, these results suggest that the triDrop is an ideal platform for cell therapy R&D and that this novel droplet EP system solves long-standing issues associated with EP leading to efficient delivery of complex payloads to hard-to-transfect cells with minimal harm.

RESULTS AND DISCUSSION

Comparing Electroporation Platforms. We analyzed three electroporation (EP) systems that are schematically overviewed in Figure S1. Figure S1a is the Invitrogen Neon Electroporation System (Neon),³² Figure S1b is the Lonza 4D-Nucleofector (NF), and Figure S1c is a recently published,³¹ droplet-based, electroporation system that relies on digital microfluidics, hereby referred to as the triDrop system. We previously demonstrated that the triDrop system is capable of inserting a range of payloads (including dextran, mRNA, DNA

plasmids, and proteins) into different cell lines (e.g., HEK293, HeLa, Jurkat, and Primary T cells) while preserving cell health by minimizing current generation (e.g., Joule heating) and harmful electrolytic byproducts during electroporation.³¹ The Neon and Nucleofector have been shown extensively for transfection of primary human T cells; however, we propose that the triDrop can offer two key advantages over these existing systems. First, is the ability to achieve high-performance transfection while using fewer cells and less payload providing up to a 20-fold reduction in the overall cost of T cell engineering (Table S1). Second, by limiting the exposure of cells to excessive electrical current and harmful electrolytic byproducts (such as pH changes as a result of the reduction and oxidation of water molecules, chlorine and hydrogen gas bubbles, and metal ions),²⁹ the health and functionality of the cells can be preserved post-electroporation. It has been shown that joule heating as a result of electrical current, and exposure to electrolysis are significant contributing factors to cell death as a result of EP,²⁸ and that cell death increases with increased joule heating and as the cells get closer to the anode and cathode.^{30,33}

Figure 1 shows that all three platforms were able to deliver mRNA molecules with efficiencies >95%. The Neon and Nucleofector achieved peak viabilities of ~65% (in line with previously published results³⁴) when using the manufacturer recommended conditions, 1×10^6 cells per reaction for Nucleofector, and 2×10^5 cells per reaction for Neon (Figure 1a,b). The triDrop had the highest reported viability as measured 18 h post-electroporation (80–85%; Figure 1c). Interestingly, reducing the number of cells per reaction results in decreasing viabilities for both the Neon and the Nucleofector, achieving ~60% and ~45% viability, respectively, for EP reactions when using only 0.5×10^5 cells per reaction. To validate the effects of using reduced cell amounts on viability, we conducted EP using either the recommended number of cells or 0.5×10^5 cells per reaction and measured viability 6 h post-EP (Figure S1d). While all systems led to a reduction in viability compared to the control, the triDrop system showed a significant improvement in viability in comparison to the Neon and Nucleofector, regardless of how many cells were used. In addition, reducing the number of cells

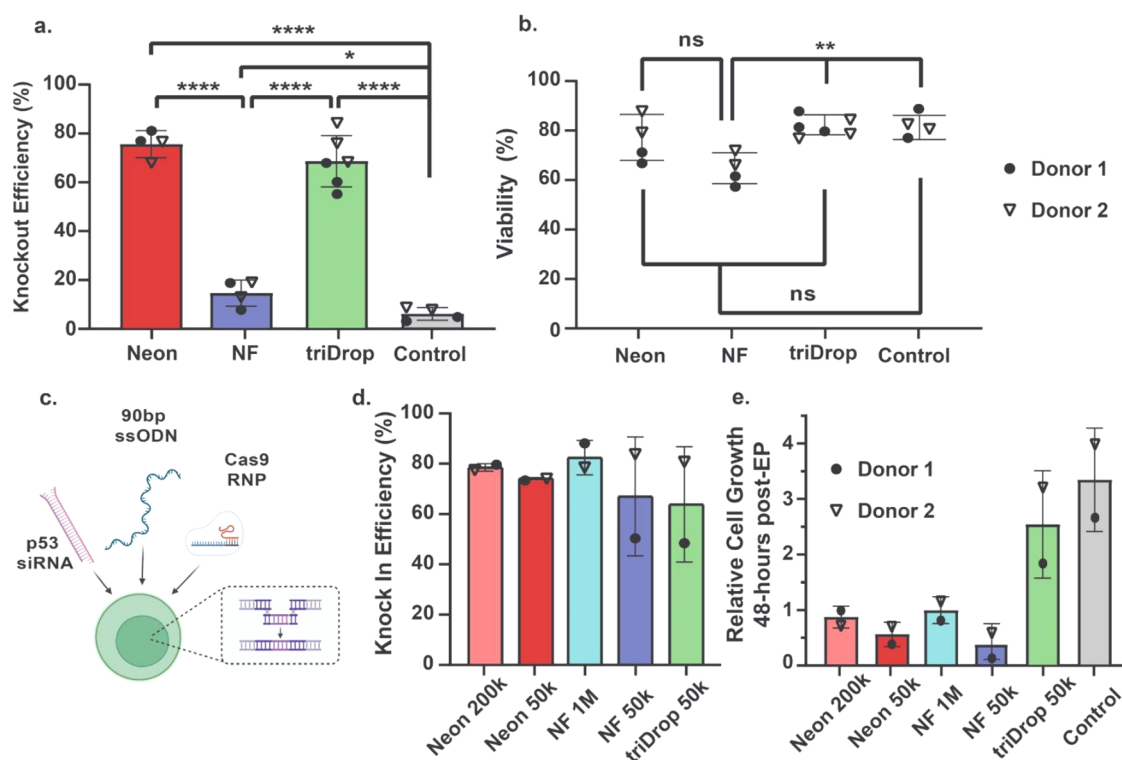


Figure 2. Gene editing. Bar graphs showing (a) knockout efficiency and (b) viability for 0.5×10^5 cells electroporated with 2.5 pmol of RNP using the three EP systems (two donors, 2–3 technical replicates). (c) Schematic showing the payloads required for CRISPR knock-in (created with BioRender.com). Bar graphs showing (d) knock-in efficiency and (e) relative cell growth post-EP for cells electroporated using manufacturer recommended number of cells or 0.5×10^5 cells per reaction (two donors). All error bars represent mean \pm 1 SD. Statistical n.s. indicates no significant difference, *, **, ***, and **** represent *p*-values below 0.05, 0.01, 0.001, and 0.0001, respectively. Statistical analysis was performed using a Student's *t* test. NF represents the Nucleofector system.

used by the Nucleofector leads to a significant reduction in viability (65 vs 51%, $P = 0.001$).

Next, we investigated the effects of using differing amounts of payload per reaction on the transfection efficiency and viability. Figure S1e–g shows line graphs depicting transfection efficiency for each condition over 72 h following EP. The Nucleofector requires approximately 10 times as much payload to achieve results comparable to the triDrop (500 vs 50 ng). Furthermore, Figure S1h shows the measured viability of each system over 72 h. The data confirms that the triDrop has the highest viability of the three systems, and by 18 h post-EP, cells treated with the triDrop have a viability of >80% compared to a viability of ~60% for the other systems (consistent with results shown in Figure 1). It is only after 72 h post-electroporation that all three systems have a recovered viability >80%.

Knockout and Knock-In Gene Editing Efficiency. A main aim of this work is to compare the electroporation systems and their performance on delivering CRISPR components directly into primary T-cells. We first investigated the performance of all three systems to conduct CRISPR knockouts targeting the T cell receptor α constant (TRAC) locus. Figure S2a–c shows the effects of knockout with all three systems using varying amounts of cells per reaction. In these experiments, ribonucleic proteins (RNP) were normalized to the reaction volume to ensure consistent payload concentration as recommended by Hultquist et al.³⁵ and Oh et al.³⁶ The triDrop achieved an optimal knockout efficiency of 75% with a viability of 80% when using 0.5×10^5 cells per reaction, and the Neon and Nucleofector were both able to

achieve knockout efficiencies ~95% when using higher numbers of cells with viabilities of 70–75%. However, decreasing cell amounts to 0.5×10^5 cells per reaction led to the efficiency dropping to 78 and 70%, respectively. These results show that the triDrop compares well against the gold standard methods for performing CRISPR knockouts while outperforming other previously shown droplet-based methods relying on viral and chemical transfection techniques.^{37,38}

Given the substantial volume differences between the three systems, adding payload in proportion to volume leads to a significant difference in the total amounts of Cas9 enzymes and sgRNA needed per reaction (i.e., 50 pmol of RNP for 1 nucleofection reaction vs 2.5 pmol for 1 triDrop reaction). To account for this difference, we tested conditions by normalizing payload to the number of cells being electroporated via addition of 50 pmol of RNP for every 1 million cells being used as recommended by Roth et al.¹² We found that when using the Nucleofector, decreasing the payload in proportion to the number of cells being electroporated led to a decrease in knockout efficiency, suggesting that volumetric normalization is more important than cellular normalization for achieving high delivery efficiency (Figure S3). Figure 2a,b, show side-by-side comparisons of two donors when electroporating only 0.5×10^5 cells with 2.5 pmol of Cas9 RNP. Both the Neon and the triDrop were able to achieve 75 and 68% knockout efficiency respectively with no significant difference between the two ($p = 0.26$), however, the Nucleofector was only able to achieve 14% knockout efficiency with these conditions, which is significantly lower than the other two systems ($p < 0.0001$). Additionally, we observed that the decreased number of cells

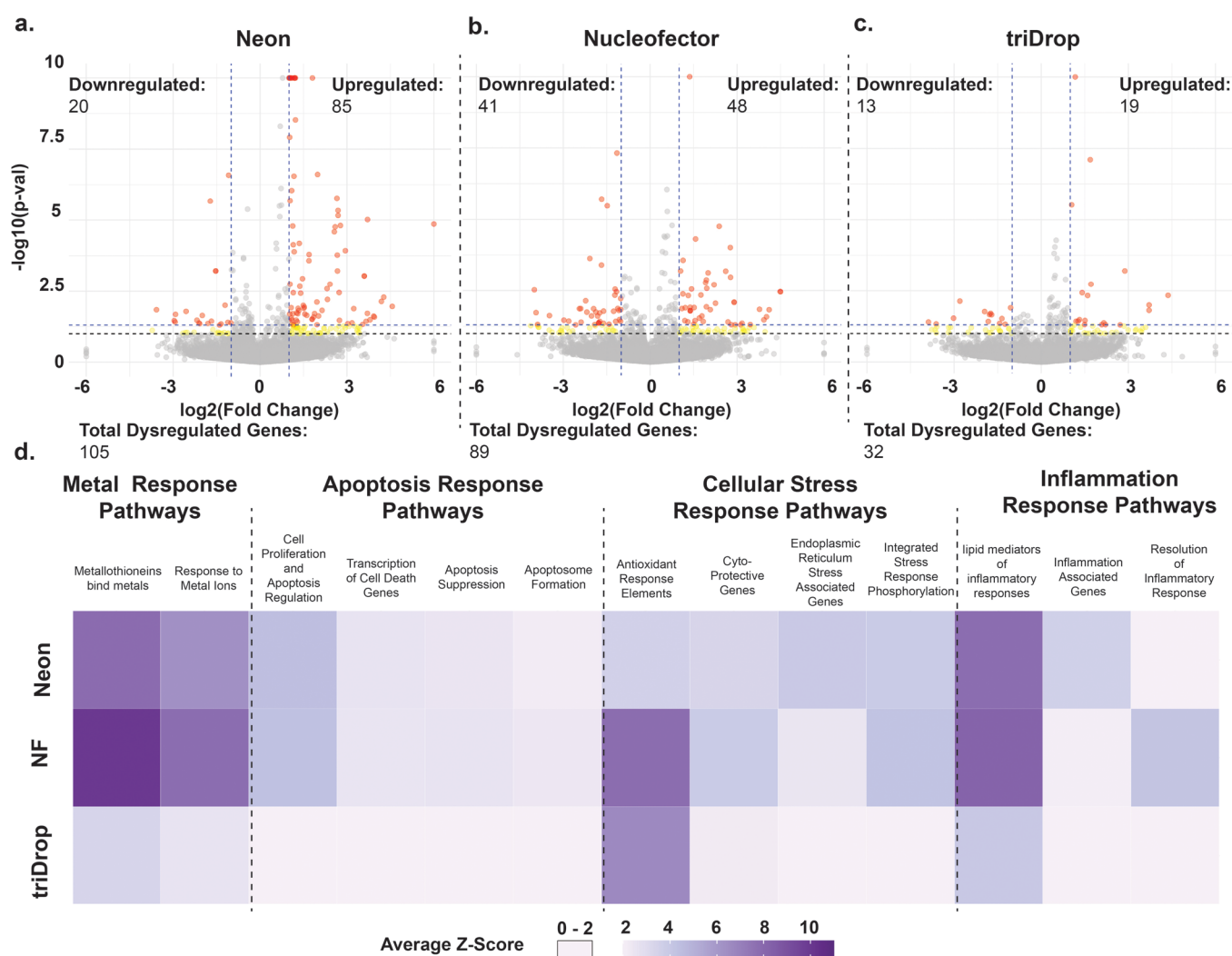


Figure 3. Transcriptomic analysis. Volcano plots depicting p -values and fold change for individual genes for cells from three different donors 6 h post-EP when electroporated with (a) Neon, (b) Nucleofactor, and (c) triDrop. Genes with a log fold change >1 or <-1 with a p value <0.05 (red dots) and <0.1 (yellow dots) are highlighted. (d) Heatmap showing the average Z-scores for 13 selected pathways for cells electroporated with all three EP systems. NF represents the Nucleofactor system.

had a significant impact on the health of cells electroporated with the Nucleofactor even after 4 days of recovery. In comparison to the control, the triDrop and Neon both had no significant differences in cell viability ($p = 0.67$ and $p = 0.3$, respectively), whereas the Nucleofactor had viabilities significantly less than both the control ($p = 0.004$) and cells treated with the triDrop ($p = 0.0008$).

After validating triDrop as a reliable method for knockout, we introduced donor templates to perform proof-of-principle CRISPR knockouts using the three methods. We followed a recent protocol published by Cloarec-Ung et al.³⁹ highlighted in Figure 2c (all sequences in Table S2). Figure 2d shows that all systems achieve average knock-in efficiencies of $>60\%$ and up to 80% insertion efficiency, which is in line with recently published results.⁴⁰ Interestingly, as shown in Figure 2e, we observed that the cells electroporated with the triDrop had proliferative capacities most similar to the control (2.5-fold increase in total viable cells vs 3.3-fold increase, respectively), and more surprisingly, Nucleofactor and Neon showed impaired proliferation post-EP. These data suggest that the triDrop offers substantial improvements in both cell viability and proliferation capacity immediately after electroporation as

well as requiring significantly less payload (at least 10-fold) and fewer cells compared to the other electroporation systems.

Transcriptomic Analysis. The triDrop was developed for the development and testing of cellular therapies. To ensure therapeutic relevance, it is essential that cells maintain their functionality and viability following electroporation. We used qPCR to look at critical cytokines (IL-2, TNF- α , and IFN- γ) in the immune system that play significant roles in cellular therapies.⁴¹ Dysregulation of these genes leads to nonspecific response or an impaired response in the presence of a target antigen.^{42,43} As shown in Figure S4, cells treated with the triDrop show no significant dysregulation in any of the three examined genes, whereas cells treated with the Neon showed a significant upregulation of IL-2 (relative fold change of 4.99, $P = 0.005$, and 5.11, $P = 0.003$) compared to the control. Similarly, when using the Nucleofactor, cells treated with the manufacturer recommended conditions showed no dysregulation of the three genes; however, when using 0.5×10^5 cells per EP reaction, IFN- γ was significantly downregulated (relative fold change of 0.38, $P = 0.0006$), indicating that cells electroporated under this condition may experience a reduced capacity to secrete this important cytokine.

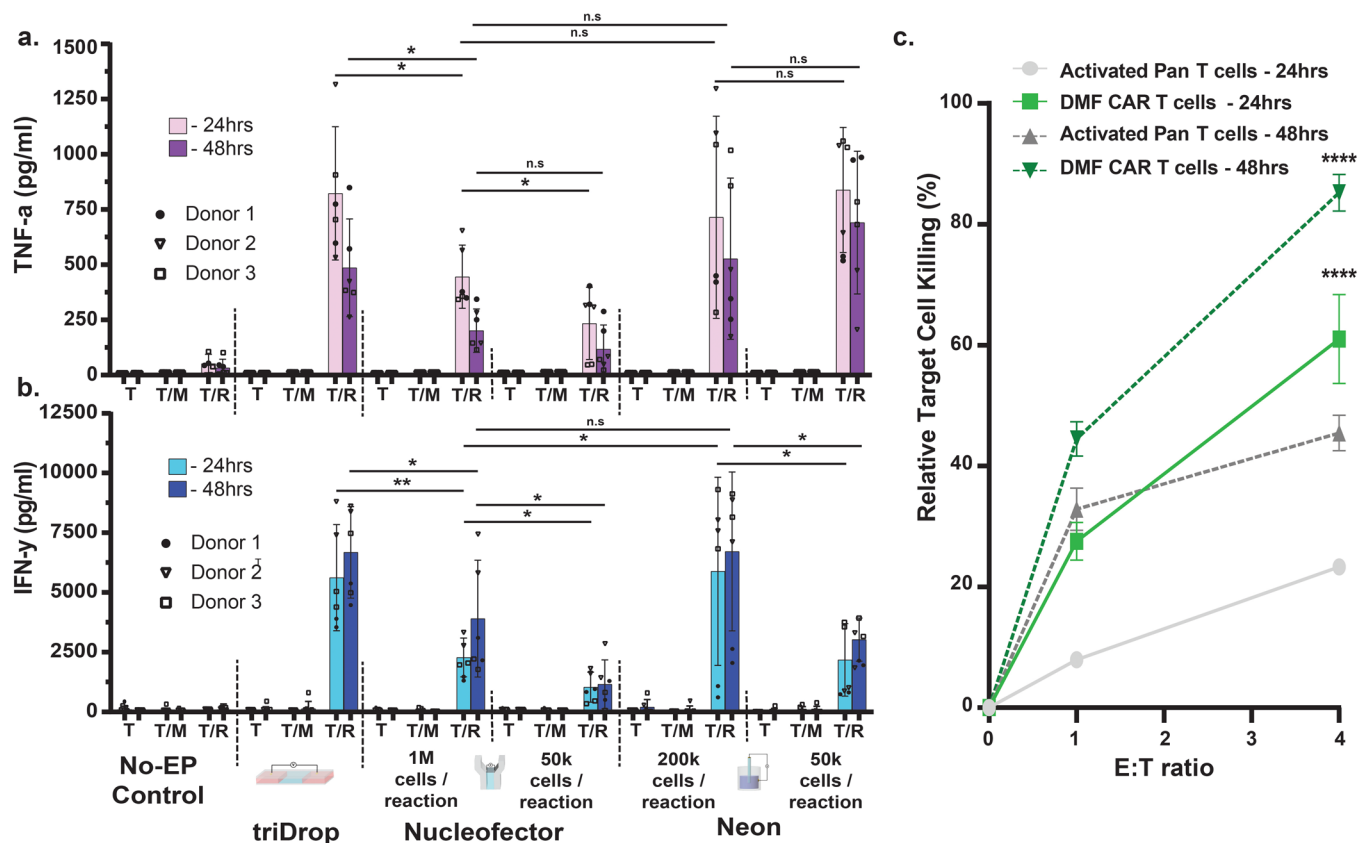


Figure 4. Functional CAR-T assays. Bar graphs depicting measured levels of (a) TNF- α and (b) IFN- γ after 24 h (light purple and light blue) and 48 h (dark purple and dark blue) of culture for cells electroporated using all three systems using either manufacturer recommended conditions or 0.5×10^5 cells per reaction. Engineered cells are cultured either by themselves (T), at a 1:1 ratio with MCF-7 cells (T/M), or with Raji cells (T/R). ($n = 6$) (c) Line graphs depicting relative killing of Raji cells cocultured with activated Pan T cells at 1:1 ratio and 4:1 ratio after 24 h (light gray, solid line) and 48 h (dark gray, dashed line) or with triDrop engineered CAR T cells at a 1:1 and 4:1 ratio after 24 h (light green, solid line), and 48 h (dark green, dashed line). Statistical significance markers indicate difference between engineered cells and activated pan T cells for each time point. ($n = 4$). All error bars represent mean \pm SD. n.s. indicates no significant difference, *, **, ***, and **** represent p-values below 0.05, 0.01, 0.001, and 0.0001, respectively. Statistical analysis was performed using a Student's *t* test.

In addition, we used RNA sequencing to examine the entire transcriptional landscape of cells treated with all three systems. Figure 3a–c shows volcano plots depicting the differential gene expression for all three electroporation systems (using manufacturer recommended conditions) compared to the control (with no electroporation). Using the cutoff metrics of >1 or <-1 log fold change and a p-value of 0.05, we sorted genes into the categories of significantly dysregulated (red dots) or nonsignificant genes (gray dots). In addition, genes meeting the less stringent condition of p-values <0.1 are shown as yellow dots. Based on these cutoffs, the Neon shows a dysregulation of 105 genes, the Nucleofector showing 89 genes, and only 32 genes for the triDrop. A principal component analysis showed triDrop to be most similar to control cells (Figure S5). To understand these results, we classified them by grouping the genes that are commonly dysregulated among the systems (Figure S6a). Six genes are commonly dysregulated among all systems and are shown in Table S3. Interestingly, 34 genes are commonly dysregulated between the Neon and the Nucleofector but not dysregulated with the triDrop. A collection of four such genes are highlighted in Figure S6b–e. The first two genes, PPP1R15A (2.7- and 2.8-fold increase for Neon and Nucleofector, respectively), and SESN2 (3.6- and 2.9-fold increase for Neon and Nucleofector, respectively), are implicated in

integrated stress response pathways with SESN2 being implicated in pathways responding to oxidative DNA damage⁴⁴ and PPP1R15A encoding for the growth arrest and DNA damage inducible protein.⁴⁵ The two other genes are TSC22D3 (2.9- and 2.4-fold change for Neon and Nucleofector, respectively) and CD48 (−1.7- and −1.4-fold change for Neon and Nucleofector, respectively) which are both known to affect the functionality of immune cells especially in the context of immunotherapy when upregulated and downregulated, respectively.^{46–49} Genes were assigned a z-score to quantify the different levels of expression relative to the control. Genes were then grouped into high-level genetic pathways using the Reactome database,⁵⁰ and the average z-score for the whole pathway was calculated. Out of the ~ 2600 pathways analyzed, the triDrop showed a dysregulation of 79 pathways (defined as a pathway with an average -score >2.0 or <-2.0), the Neon with 130, and the Nucleofector showing 134. Figure 3d summarizes a collection of pathways that are further documented in Table S4. All systems upregulate pathways responding to metal ion contamination (possibly secreted from the anode and cathode), with the lowest z-score shown by the triDrop. Additionally, the Neon and the Nucleofector upregulate pathways corresponding to apoptosis and cellular stress, which may further explain earlier data showing reduced viabilities and proliferation capabilities for

cells treated with these systems. Finally, we observed upregulation of three inflammation pathways that are minimally upregulated or not upregulated with the triDrop. Upregulation of these pathways may lead to premature T cell exhaustion⁵¹ which can impair the function of immunotherapeutic T cells.⁵²

Functional CAR-T Assays. To demonstrate the potential of our system for engineering CAR-T cells, we present for the first time the use of a DMF platform to generate functional cell therapies. Primary human T cells were engineered to express an anti-CD19 CAR molecule (Figure S7a). Figure S7b shows the expression of the anti-CD19 CAR protein with all three of the tested EP systems being able to achieve >80% expression of the CAR protein 6 h post-EP. Expression peaked at 24 h, then slowly declined over the subsequent 2 days (Figure S7c). Anti-CD19 CAR expression via electroporation was as efficient as viral methods^{53,54} (60–80.6%) and chemical⁵⁵ (84.6%) methods. However, the use of electroporation does not require the need to produce viral particles or lipid nanoparticles, indicating that electroporation is a more convenient approach for CAR-T R&D.

To test the functionality of the engineered cells, anti-CD19 CAR-T cells were cultured by themselves or cocultured with either MCF-7 cells (CD19-negative) or Raji cells (CD19-positive) at a 1:1 ratio. Figure 4a,b show bar graphs depicting the cytokine levels of IFN- γ and TNF- α in the supernatant for cells under various treatments and culture conditions after 24 and 48 h of coculture. Importantly, none of the engineered cells produced either of the antitumor cytokines when cultured by themselves or in the presence of CD19-negative cells, indicating a highly specific response of the anti-CD19 CAR. Impressively, when cultured with CD19-positive targets, cells engineered with the triDrop were capable of secreting approximately 2-fold more antitumor cytokines compared to cells engineered with the Nucleofector when using manufacturer recommended conditions. We observed increased production of both IFN- γ (24 h: $p = 0.006$, 48 h: $p = 0.05$), and TNF- α (24 h: $p = 0.02$, 48 h: $p = 0.016$). Cells engineered with the Neon also have higher cytokine production than Nucleofected cells but lack statistical significance across the 24 and 48 h time points. Additionally, using 0.5×10^5 cells per reaction with the Nucleofector led to a significant reduction in cytokine production capabilities producing ~ 2 -fold less cytokines than cells treated with the manufacturer recommended conditions and ~ 5 -fold less than cells engineered with the triDrop. These data suggest that the Nucleofector impairs immune function immediately following EP (as seen by the transcriptional sequencing data) and that attempting to use fewer cells than recommended by the manufacturer further exacerbates this impairment. While the Neon was able to produce similar average levels of cytokines compared to triDrop, the response was highly variable across donors. Further, similar to the Nucleofector, using 5×10^5 cells per reaction with the Neon surprisingly led to a significant reduction in the cells' ability to produce IFN- γ (although not TNF- α).

Finally, we test the ability to use cells engineered with our triDrop platform for killing Raji cells in coculture. Figure 4c shows, as expected, that the activated Pan T cells elicit a small cytotoxic effect on the Raji cells, leading to $\sim 23\%$ (24 h) and 45% (48 h) killing of target cells when cocultured at the 4:1 effector-to-target ratio. However, when cocultured with the triDrop engineered CAR T cells, approximately 27% (24 h)

and 45% (48 h) of target cells are killed when cultured at a 1:1 ratio and 61% (24 h) and 85% (48 h) are killed at a 4:1 effector:target ratio indicating a robust killing effect.

CONCLUSIONS

In this work, we demonstrated that our miniaturized droplet electroporation system allows for a substantial reduction in the consumption of expensive reagents and precious cells compared to two state-of-the-art electroporation systems. We propose that this advancement will allow for a reduction in the cost of gene editing making cell therapy R&D more affordable, or alternatively making it possible to screen large libraries of edits on rare cell populations or cells from a single donor. Additionally, we showed that the triDrop structure achieved on our DMF platform allows us to protect cells from the harmful effects of joule heating and electrochemical reactions that occur during the electroporation process and that this results in cells with less transcriptional dysregulation and, most importantly, improved functionality when compared to cells electroporated using traditional methods. Given DMF's capability to seamlessly interface with existing lab automation paradigms, we predict this method will facilitate large-scale arrayed screens to help identify next-generation genetic modifications to improve immunotherapeutic outcomes.

MATERIALS AND METHODS

DMF device fabrication and assembly, droplet operations, and the electroporation circuit (Figure S8) are described in the Supporting Information.

Electroporation. For all electroporation platforms, primary human T cells were electroporated within 24 h after the removal of activation beads. Cells were in electroporation buffer for a maximum of 15 min and were transferred to recovery buffer (culture media containing 400 IU/mL IL-2) promptly after pulse application using one of the three systems. For both the Neon and Nucleofector, a wide range of pulse parameters (voltage amplitude, number of pulses, and pulse duration) have been shown for effective electroporation. In this work, we use the pulse parameters recommended by the manufacturer for working with activated primary human T cells^{56,57} and shown to be effective by Zhang et al.⁵⁸ and Schumann et al.⁵⁹ which are 3, 1600 V_{DC} pulses, and 10 ms in duration for the Neon and pulse code EO-115 for the Nucleofector.

Transfection efficiency is defined as the ratio of positively transfected cells relative to total living cells as measured using flow cytometry, eq 1

$$TE = \frac{\text{number of transfected living cells}}{\text{total number of living cells}} \times 100 \quad (1)$$

Knock-In. 48 h post-electroporation, genomic DNA (gDNA) was recovered from the cells using the DNeasy Blood and Tissue Kit (Qiagen, Catalog #69504). gDNA was amplified using 0.5 μM of pri077F+R primers (Table S2) with the following thermal cycle: 98 $^\circ\text{C}$ 30s; 35 \times (98 $^\circ\text{C}$ 10s, 60 $^\circ\text{C}$ 10s, 72 $^\circ\text{C}$ 30s); 72 $^\circ\text{C}$ 5 min. Following amplification, PCR products were purified with the GeneJET PCR purification kit (Thermo Fisher, Catalog #K0702). Purified PCR products were quantified by NanoDrop at a range of 20–40 ng/ μL , and 5–15 ng was sent for Sanger sequencing at the IRC Genomics core with the primer pri0003-A1 (Table S2). Chromatograms for each condition were aligned against a control sample using

SnapGene's alignment tool and validated with Synthego's ICE Analysis (Figure S9).

Transcriptomic Sequencing and Analysis. Base calling was performed using Oxford Nanopore's Dorado software. Sequencing reads were aligned with the *Homo sapiens* GRCh38 transcriptome using Minimap2.⁶⁰ Transcript counts were performed using Salmon⁶¹ and mapped to genomic data using the R/Bioconductor package biomaRt.⁶² Differential expression was calculated using DESeq2.⁶³ Z scores were used to quantify variation from the control based on the number of transcripts per million (TPM) that were counted for each gene using eq 2

$$Z_{\text{score}} = \frac{\text{TPM}_{\text{treated}} - \text{TPM}_{\text{control}}}{\text{SD}_{\text{control}}} \quad (2)$$

Genes were grouped into high-level genetic pathways using the Reactome database⁵⁰ and analyzed using the ReactomePA package.⁶⁴ When performing pathway enrichment analysis using the Reactome database, we execute the enrichment simplify() function, which reduces redundancy in pathways using semantic similarity metrics. Such a function sets a similarity threshold (biological categories that are considered redundant; cutoff = 0.7) and keeps the pathway by the lowest-adjusted *p*-value (by = "p.adjust" and select-fun = "min").

CAR-T Assays. Four hours prior to the tumor cell killing assay, 2.5×10^4 Raji cells per well were seeded in a U-bottom well plate in 100 μL of fresh Roswell Park Memorial Institute (RPMI) media with 10% FBS and 2.5×10^4 MCF-7 cells per well were seeded in a treated flat-bottom 96-well plate in 100 μL of fresh RPMI with 10% FBS. Control wells were seeded with 100 μL of fresh RPMI containing no cells.

After 6 h of recovery, electroporated and control cells were counted, washed in PBS, and resuspended in fresh RPMI with 10% FBS at a concentration of 2.5×10^4 cells per 100 μL . 100 μL of cell solution from each condition was then added in technical replicates to wells prepared earlier containing either just media, MCF-7 cells, or Raji cells. Supernatant was collected after 24 and 48 h by centrifuging the plates for 3 min at 300g to pellet the cells and pipetting 180 μL from the top of each well. Supernatant was analyzed via ELISA using the manufacturer recommended protocol for INF- γ (BD Biosciences, catalog #555142) and TNF- α (BD Biosciences, catalog #555212).

Tumor cell killing was performed by coculturing CAR T cells or control activated Pan T cells with Raji cells at a 1:1 (2.5×10^4 T cells: 2.5×10^4 Raji cells) or 4:1 ratio (1×10^5 T cells: 2.5×10^4 Raji cells). Raji cell death was validated via flow cytometry using previously established methods.⁶⁵ After 24 h of coculture, cells are recovered and washed before being stained with PE-CD3 monoclonal antibody and prepared for flow cytometry. Immediately before flow cytometry, 4',6-diamidino-2-phenylindole (DAPI) is added to visualize cell viability. PE-CD3 staining allows for differentiation between T cells and Raji cells, and DAPI allows for the visualization of living and dead cells. A detailed gating overview is shown in Figure S10. Relative killing efficiency was measured using eq 3

$$\eta_{\text{killing}} = \left[1 - \left(\frac{\text{target cell viability}_{\text{treated}}}{\text{target cell viability}_{\text{untreated}}} \right) \right] \times 100 \quad (3)$$

where treated target cell viability represents the viability of Raji cells cocultured with either activated Pan T cells or CAR T cells, and untreated viability represents the viability of Raji cells cultured by themselves under the same conditions over the same period.

■ ASSOCIATED CONTENT

Data Availability Statement

Data for this article are available at Open Science Framework at DOI: 10.17605/OSF.IO/8NS6G. The repository is titled "A Digital Microfluidic Platform for the Microscale Production of Functional Immune Cell Therapies".

Supporting Information

The Supporting Information is available free of charge at <https://pubs.acs.org/doi/10.1021/acs.analchem.4c06911>.

Methods for device fabrication, cell culturing of Primary T cells and immortalized cell lines, transfection, genetic analysis (RT-qPCR, RNaseq, flow cytometry); tables showing cost comparison, genetic/qPCR primer sequences, dysregulated genes, reactome pathway analysis; figures showing three electroporation systems, knockout analysis, payload analysis, qPCR analysis, RNaseq data, dysregulated gene analysis, CAR-T functional assay, triDrop electroporation circuit schematic, sequencing chromatograms, CAR killing flow cytometry pipeline analysis (PDF)

■ AUTHOR INFORMATION

Corresponding Author

Steve C. C. Shih – Department of Electrical and Computer Engineering, Concordia University, Montréal, Québec H4B 1R6, Canada; Centre for Applied Synthetic Biology and Department of Biology, Concordia University, Montréal, Québec H4B 1R6, Canada; orcid.org/0000-0003-3540-0808; Email: steve.shih@concordia.ca

Authors

Samuel R. Little – Department of Electrical and Computer Engineering, Concordia University, Montréal, Québec H4B 1R6, Canada; Centre for Applied Synthetic Biology, Concordia University, Montréal, Québec H4B 1R6, Canada

Niloufar Rahbari – Centre for Applied Synthetic Biology, Concordia University, Montréal, Québec H4B 1R6, Canada; Department of Chemical Engineering, Concordia University, Montréal, Québec H4B 1R6, Canada

Mehri Hajiaghayi – Department of Biology, Concordia University, Montréal, Québec H4B 1R6, Canada

Fatemeh Gholizadeh – Department of Biology, Concordia University, Montréal, Québec H4B 1R6, Canada

Fanny-Mei Cloarec-Ung – Institut de Recherche en Immunologie et en Cancérologie, Université de Montréal, Montréal, Québec H3T 1J4, Canada

Joel Phillips – Department of Biology, Concordia University, Montréal, Québec H4B 1R6, Canada

Hugo Sinha – Drop Genie, Inc., Boston, Massachusetts 02111, United States

Alison Hirukawa – Drop Genie, Inc., Boston, Massachusetts 02111, United States

David J.H.F. Knapp – Institut de Recherche en Immunologie et en Cancérologie, Université de Montréal, Montréal, Québec H3T 1J4, Canada; Département de Pathologie et Biologie

Cellulaire, Université de Montréal, Montréal, Québec H3T 1J4, Canada

Peter J. Darlington – Department of Biology, Concordia University, Montréal, Québec H4B 1R6, Canada

Complete contact information is available at:

<https://pubs.acs.org/10.1021/acs.analchem.4c06911>

Author Contributions

Experiments were designed by S.R.L. and S.C.C.S. S.R.L. and N.R. performed transcriptomic analysis. N.R. and J.P. designed qPCR primers, qPCR was optimized and performed by N.R. DMF control software along with electroporation hardware and software were developed by S.R.L. F.G., M.H., and P.J.D. developed the methodology for cell isolation and freezing from fresh blood, and F.G. and M.H. performed the isolation and freezing protocols as well as all ELISAs. F.M.C.U. and D.J.H.F.K. developed CRISPR knock-in methodology. S.C.C.S. secured required funding for the project. S.R.L. and S.C.C.S. wrote the manuscript which was revised and reviewed by all authors.

Notes

The authors declare no competing financial interest.

S.R.L., A.H., and S.C.C.S. are co-inventors on a patent application related to the triDrop structure (Systems and methods for applying voltages within droplet-based systems; PCT US2022/032083) that describes the liquid structures for transfection reported here. A.H. and H.S. are employees of Drop Genie, Inc. that is commercializing the triDrop structure. The remaining authors declare no competing interest.

ACKNOWLEDGMENTS

We thank the Natural Sciences and Engineering Research Council (NSERC), the Fonds de Recherche Nature et Technologies (FRQNT), the Canadian Foundation of Innovation (CFI), and MEDTEQ for funding. S.R.L. thanks NSERC CGS-D for funding. N.R. and S.C.C.S. thank the School of Health at Concordia University for funding. S.R.L. and N.R. thank Concordia University Department of Electrical and Computer Engineering for FRS funding. S.C.C.S. thanks Concordia University for a Research Chair. F.M.C.U. and D.J.H.F.K. thank the Terry Fox Research Institute (Terry Fox New Investigator Award #TFRI 1118). D.J.H.F.K. has salary support from FRQS in the form of a Chercheurs-boursiers Junior 1 fellowship (#283502). F.M.C.U. was supported by a Cole Foundation Doctoral Award, a bourse d'excellence du programme de biologie moléculaire from the Université de Montréal and a PhD scholarship from the Institut de Recherche en Immunologie et en Cancérologie.

REFERENCES

- (1) Finck, A. V.; Blanchard, T.; Roselle, C. P.; Golinelli, G.; June, C. H. *Nat. Med.* **2022**, *28*, 678–689.
- (2) Stadtmauer, E. A.; Fraietta, J. A.; Davis, M. M.; et al. *Science* **2020**, *367*, No. eaba7365.
- (3) Scholler, J.; Brady, T. L.; Binder-Scholl, G.; et al. *Sci. Transl. Med.* **2012**, *4*, No. 132ra53.
- (4) June, C. H.; Sadelain, M. *N. Engl. J. Med.* **2018**, *379*, 64–73.
- (5) Patel, U.; Abernathy, J.; Savani, B. N.; et al. *eJHaem* **2022**, *3*, 24–31.
- (6) Kennedy, L. B.; Salama, A. K. S. *CA Cancer J. Clin.* **2020**, *70*, 86–104.
- (7) Hyrenius-wittsten, A.; Su, Y.; Park, M.; et al. *Sci. Transl. Med.* **2021**, *13*, No. eabd8836.

- (8) Wellhausen, N.; Agarwal, S.; Rommel, P. C.; Gill, S. I.; June, C. H. *Curr. Opin. Immunol.* **2022**, *74*, 76–84.
- (9) Ellis, G. I.; Sheppard, C. N.; Riley, L. J. *Nat. Rev. Genet.* **2021**, *22*, 427–447.
- (10) Dodson, B. P.; Levine, A. D. *BMC Biotechnol.* **2015**, *15*, No. 70.
- (11) Gurusamy, D.; et al. *Cancer Cell* **2020**, *37*, 818–833.
- (12) Roth, T. L.; Puig-Saus, C.; Yu, R.; et al. *Nature* **2018**, *559*, 405–409.
- (13) Sharei, A.; Trifonova, R.; Jhunjunwala, S.; et al. *PLoS One* **2015**, *10*, No. e0118803.
- (14) Hur, J.; Park, I.; Lim, K. M.; et al. *ACS Nano* **2020**, *14*, 15094–15106.
- (15) Joo, B.; Hur, J.; Kim, G. B.; Yun, S. G.; Chung, A. J. *ACS Nano* **2021**, *15*, 12888–12898.
- (16) Li, J.; Wang, B.; Juba, B. M.; et al. *ACS Chem. Biol.* **2017**, *12*, 2970–2974.
- (17) Loo, J.; Sicher, I.; Goff, A.; et al. *Sci. Rep.* **2021**, *11*, No. 21407.
- (18) Jarrell, J. A.; Twite, A. A.; Lau, K. H. W. J.; et al. *Sci. Rep.* **2019**, *9*, No. 3214.
- (19) Sevenler, D.; Toner, M. *Nat. Commun.* **2024**, *15*, No. 115.
- (20) Lissandrello, C. A.; Santos, J. A.; Hsi, P.; et al. *Sci. Rep.* **2020**, *10*, No. 18045.
- (21) Jayasooriya, V.; Ringwelski, B.; Dorsam, G.; Nawarathna, D. *Lab Chip* **2021**, *21*, 3748–3761.
- (22) Kim, H.; Kim, S.; Lim, H.; Chung, A. J. *Lab Chip* **2024**, *24*, 1088–1120.
- (23) Hur, J.; Chung, A. J. *Adv. Sci.* **2021**, *8*, No. 2004595.
- (24) Weaver, A. N.; Iams, W. T.; Park, J. C.; et al. *Mol. Carcinog.* **2024**, *63*, 1421–1428.
- (25) Campelo, S. N.; Huang, P.-H.; Buie, C. R.; Davalos, R. V. *Annu. Rev. Biomed. Eng.* **2023**, *25*, 77–100.
- (26) DiTommaso, T.; Cole, J. M.; Cassereau, L.; et al. *Proc. Natl. Acad. Sci. U.S.A.* **2018**, *115*, E10907–E10914.
- (27) Hur, J.; Kim, H.; Kim, U.; et al. *Nano Lett.* **2023**, *23*, 7341–7349.
- (28) Rols, M.-P. Parameters Affecting Cell Viability Following Electroporation In Vitro. In *Handbook of Electroporation*; Springer, 2017; Vol. 75, pp 1449–1465.
- (29) Saulis, G.; Lape, R.; Pranevičiute, R.; Mickevičius, D. *Bioelectrochemistry* **2005**, *67*, 101–108.
- (30) Li, Y.; Wu, M.; Zhao, D.; et al. *Sci. Rep.* **2016**, *5*, No. 17817.
- (31) Little, S. R.; Leung, Z.; Quach, A. B.; et al. *Adv. Mater. Technol.* **2023**, *8*, No. 2300719.
- (32) Kim, J. A.; Cho, K.; Shin, M. S.; et al. *Biosens. Bioelectron.* **2008**, *23*, 1353–1360.
- (33) Hoffman, A. G. Animal Cell Electroporation And Electrofusion Protocols: Instrumentation. In *Cell Electroporation Electrofusion Protocol*; Springer, 1995; Vol. 3, pp 41–59.
- (34) Aksoy, P.; Aksoy, B. A.; Czech, E.; Hammerbacher, J. Viable and efficient electroporation-based genetic manipulation of unstimulated human T cells *bioRxiv* 2018.
- (35) Hultquist, J. F.; Hiatt, J.; Schumann, K.; et al. *Nat. Protoc.* **2019**, *14*, 1–27.
- (36) Oh, S. A.; Seki, A.; Rutz, S. *Curr. Protoc. Immunol.* **2019**, *124*, No. e69.
- (37) Sinha, H.; Quach, A. B. V.; Vo, P. Q. N.; Shih, S. C. C. *Lab Chip* **2018**, *18*, 2300–2312.
- (38) Quach, A. B. V.; Little, S. R.; Shih, S. C. C. *Anal. Chem.* **2022**, *94*, 4039–4047.
- (39) Cloarec-Ung, F. M.; et al. *eLife* **2023**, *12*, No. RP91288.
- (40) Shy, B. R.; Vykunta, V. S.; Ha, A.; et al. *Nat. Biotechnol.* **2023**, *41*, 521–531.
- (41) Mejía-Guarnizo, L. V.; Monroy-Camacho, P. S.; Turizo-Smith, A. D.; Rodríguez-García, J. A. *Front. Immunol.* **2023**, *14*, No. 1298571.
- (42) Gocher, A. M.; Workman, C. J.; Vignali, D. A. A. *Nat. Rev. Immunol.* **2022**, *22*, 158–172.
- (43) Ward-Kavanagh, L. K.; Lin, W. W.; Šedý, J. R.; Ware, C. F. *Immunity* **2016**, *44*, 1005–1019.

- (44) Garaeva, A. A.; Kovaleva, I. E.; Chumakov, P. M.; Alexandra, G. *Cell Cycle* **2016**, *15*, 64–71.
- (45) Magg, V.; Manetto, A.; Kopp, K.; et al. *Cell Rep.* **2024**, *43*, No. 114069.
- (46) Bereshchenko, O.; et al. *Front. Pharmacol.* **2019**, *10*, No. 308.
- (47) Yang, H.; Xia, L.; Chen, J.; et al. *Nat. Med.* **2019**, *25*, 1428–1441.
- (48) Hong, C.; Choi, Y. H.; Wald, D.; Hwang, T. H. *J. Immunother. Cancer* **2023**, *11*, No. 1322.
- (49) Mcardel, S. L.; Terhorst, C.; Sharpe, A. H. *Clin. Immunol.* **2016**, *164*, 10–20.
- (50) Croft, D.; Mundo, A. F.; Haw, R.; et al. *Nucleic Acids Res.* **2014**, *42*, 472–477.
- (51) Wherry, E. J. *Nat. Immunol.* **2011**, *12*, 492–499.
- (52) Gumber, D.; Wang, L. D. *eBioMedicine* **2022**, *77*, No. 103941.
- (53) Ghassemi, S.; Durgin, J. S.; Nunez-Cruz, S.; et al. *Nat. Biomed. Eng.* **2022**, *6*, 118–128.
- (54) Tumaini, B.; et al. *Cytotherapy* **2014**, *15*, 1406–1415.
- (55) Kitte, R.; et al. *Mol. Ther.–Methods Clin. Dev.* **2023**, *31*, No. 101139.
- (56) CRISPR/Cas9-mediated Genome Editing of Human Primary T-cells using the Neon™ Transfection System.
- (57) Amaxa™ 4D-Nucleofector™ Protocol for stimulated Human T Cells For 4D-Nucleofector™ X Unit.
- (58) Zhang, J.; Hu, Y.; Yang, J.; et al. *Nature* **2022**, *609*, 369–374.
- (59) Schumann, K.; Lin, S.; Boyer, E.; et al. *Proc. Natl. Acad. Sci. U.S.A.* **2015**, *112*, 10437–10442.
- (60) Li, H. *Bioinformatics* **2018**, *34*, 3094–3100.
- (61) Patro, R.; Duggal, G.; Love, M. I.; Irizarry, R. A.; Kingsford, C. *Nat. Methods* **2017**, *14*, 417–418.
- (62) Durinck, S.; Spellman, P. T.; Birney, E.; Huber, W. *Nat. Protoc.* **2009**, *4*, 1184–1191.
- (63) Love, M. I.; Huber, W.; Anders, S. *Genome Biol.* **2014**, *15*, No. 550.
- (64) Yu, G.; He, Q.-Y. *Mol. Biosyst.* **2016**, *12*, 477–479.
- (65) Kiesgen, S.; Messinger, J. C.; Chintala, N. K.; Tano, Z.; Adusumilli, P. S. *Nat. Protoc.* **2021**, *16*, 1331–1342.